Geosynchronous Sar Moving Target Detection And Motion Parameters Estimation using the Non Uniform Cubic Phase Function Algorithm

Mounir Melzi, Cheng Hu, Xichao Dong, Chang Cui
Department of Electronic Engineering
Beijing Institute of Technology
Beijing, China
melzi_m@bit.edu.cn

***Abstract* — This paper addresses the issue of moving target detection and velocity estimation in the Geosynchronous Synthetic Aperture Radar (GEO SAR) scenario, this problem has not been handled yet despite the promising potential of GEO SAR systems in the global monitoring domain. New expressions for the Doppler centroid and the Doppler rate that take into account the specific features of a geosynchronous orbit are developed. Moreover, a new Ground Moving Target Indication (GMTI) technique was proposed, it makes use of the aforementioned expressions combined with the use of the Non Uniform Cubic Phase Function (NUCPF) algorithm to estimate the moving target motion parameters. Simulation results are carried out to demonstrate the accuracy of the developed expressions and the effectiveness of the proposed GEO SAR GMTI technique.**

Keywords — Geosynchronous Synthetic Aperture Radar (GEO SAR), Ground Moving Target Indication (GMTI), Cubic Phase Function (CPF).

I. INTRODUCTION

Moving target detection and velocity estimation has drawn a lot of interest due to their importance in many civilian and military Synthetic Aperture Radar (SAR) applications [1][2], various techniques have been developed to tackle this issue. Yet, these tools have been set to address the Ground Moving Target Indication (GMTI) problem in the case of a Low-Earth Orbit Synthetic Aperture Radar (LEO SAR) and airborne SAR situations, but no such technique deals with Geosynchronous Orbit SAR (GEO SAR) imaging scenarios. Furthermore, GEO SAR systems have gained more attention recently, especially with the increase need for a more global monitoring of the earth's surface, and the recent technological achievements that make it possible in the near future to put a GEO SAR satellite on orbit. In addition, Most of the algorithms that address the GMTI problem need two or more antennas to take advantage of the along-track SAR data: Space-Time Adaptive Processing (STAP)[3][4], mono-pulse processing [5], Displaced Phase Centre Array (DPCA) [6] or along track interferometry (ATI) [7]. For these multichannel-based techniques to work well, some limitations related to the acquisition process must be fulfilled, such as linear SAR sensor trajectory [8] and a constant platform velocity. However, in the GEO SAR scenario, the satellite velocity changes because of the sensor curved trajectory [9], which may impact the efficiency of the algorithm. On the other hand, the use of a single channel GMTI remains a simple and cheaper solution to solve the GMTI problem in the GEO SAR case. Its use is made possible thanks to the singular Doppler characteristics of a GEO SAR system that are different from the LEO SAR one, in fact, the GEO SAR satellite moves around the earth in a synchronous way leading to a rather small satellite velocity with respect to the earth, which has the effect of shrinking the azimuth frequency support of both stationary (clutter) and moving targets, and thus facilitating the separation between their spectrums.

In this work, we first develop closed-form expressions of the moving target Doppler parameters (Doppler centroid, Doppler rate) with respect to its motion parameters (velocity, acceleration) in the GEO SAR scenario, since the existing expressions that relates these two Doppler aspects in the LEO SAR case are no longer valid, because of the satellite curved trajectory, the long exposure time, and the high satellite orbit [10]. Having these new relations set, we use the Non Uniform Cubic Phase Function (NUCPF) algorithm to estimate the Doppler parameters of the compressed band-pass filtered azimuth signal, and then deduce the target motion parameters.

The remainder of this paper is organized as follows, in section II, the problem of Doppler ambiguity usually encountered in single channel SAR GMTI is analysed in the GEO SAR scenario. Section III provides a new formulation for a moving target Doppler centroid and Doppler rate with respect to its motion parameters, in the GEO SAR situation; the NUCPF technique, used for the Doppler parameters estimation is described in section IV. Section V presents the simulation results and conclusions are detailed in section VI.

II. DOPPLER AMBIGUITY IN GEO SAR

In GEO SAR, the Clutter Doppler bandwidth is given as follows [1]:

$$\Delta f_{dop} = \frac{2v_{sa}}{\lambda} cos(\theta_{sq})\, \delta_{bw} \tag{1}$$

where:

Δf_{dop} is the Clutter Doppler bandwidth, v_{sa} is the satellite ground velocity in the azimuth direction, λ is the wavelength, $\delta_{bw} = \frac{\lambda}{L_{ant}}$, is the satellite azimuth beamwidth, where L_{ant} represents the sensor's real aperture in the azimuth direction and θ_{sq} is the squint angle. Replacing the expression of the satellite azimuth beamwidth into (1) and assuming a zero squint angle (broadside mode), we get:

$$\Delta f_{dop} = \frac{2v_{sa}}{L_{ant}} \quad (2)$$

From the above equation, we can see that the small velocity of the satellite with respect to the earth combined with the long antenna's aperture in the GEO SAR [1][11], results in a smaller Doppler bandwidth, which broadens the Doppler support where moving targets can be detected compared to the LEO SAR case. To illustrate that effect, we simulate in the following, a moving target immersed in a background Clutter in both LEO SAR and GEO SAR scenarios, and present the corresponding Doppler spectrums. The STK9 software was used to simulate the two scenarios where the GEO orbit is a small '8' generated using the parameters in Table I. The parameters used for the SAR imaging are given in Table II and the corresponding results are given in Fig.1.

We can notice from Fig.1 the big difference in the Clutter Doppler bandwidth between the two scenarios, and the large Doppler support available in the GEO SAR case where targets can be detected and their motion parameters estimated without ambiguity.

III. GEO SAR MOVING TARGET DOPPLER PARAMETERS

In order to use the Doppler parameters in the estimation of the moving target motion parameters, we first need to extract the new relations that link these two set of variables (Doppler and motion parameters) in the GEO SAR case, where a long exposure time and a higher orbit altitude, affect seriously the SAR mapping process. In fact, the long exposure time alters the accuracy of the "stop-and-go" assumption, that prevails for the LEO SAR imaging [12]. In addition, the lower satellite velocity due to the geosynchronous movement induces a long integration time, which affects the ability of the hyperbolic model to fit the slant range history [10].

The baseband received signal from a moving target is given as:

$$S(t_a) = A.exp\left(-j2\pi f_0 \frac{R(nT)}{c}\right) rect\left(\frac{t_a}{T_e}\right) \quad (3)$$

Where A is complex amplitude that accounts for the fast time compressed signal pattern, azimuth pattern and target's reflectivity, $R(nT)$ is the target's range at time n, f_0 is the carrier frequency, c is the light speed, $T = \frac{1}{PRF}$, is the azimuth sampling time, t_a is the slow time, and T_e is the targets exposure time.

We first deduce the expression of the moving target range by considering the "stop-and-go" error generated during one azimuth Pulse Repetition Interval (PRI) [12].

Let consider $R_n(t_r)$, where n represents the slow time and t_r the fast time.

The target-satellite two- way propagation range signal during a single PRI (n) (considering an Earth Centered Earth Fixed (ECEF) frame) can be expressed as (see Fig.2):

TABLE I. GEO ORBIT SIMULATION PARAMETERS

Semi major Axis	42164 km
Eccentricity	0
Inclination	16°
Argument of Perigee	—
Longitude of Ascending Node	88°

TABLE II. SAR IMAGING PARAMETERS

Parameters	GEO SAR	LEO SAR
PRF	400 Hz	6.5 KHz
Carrier frequency f_0	1.25 GHz	9.65 GHz
Fast time bandwidth B	18 MHz	150 MHz
Fast time pulse width T_p	20 μs	20 μs
Antenna aperture D	30m	4.8m

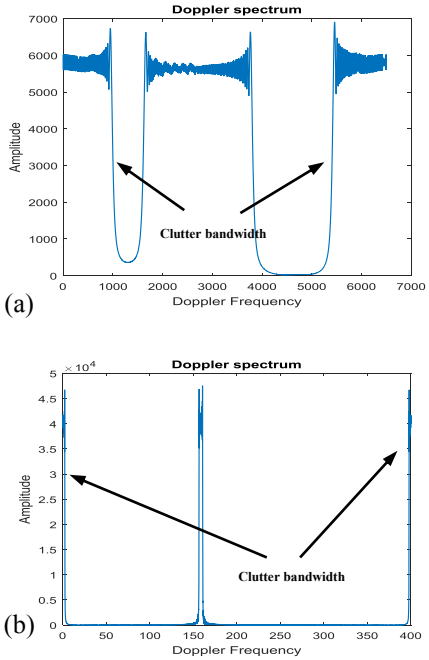

Fig. 1. (a) LEO SAR Doppler spectrum, (b) GEO SAR Doppler spectrum.

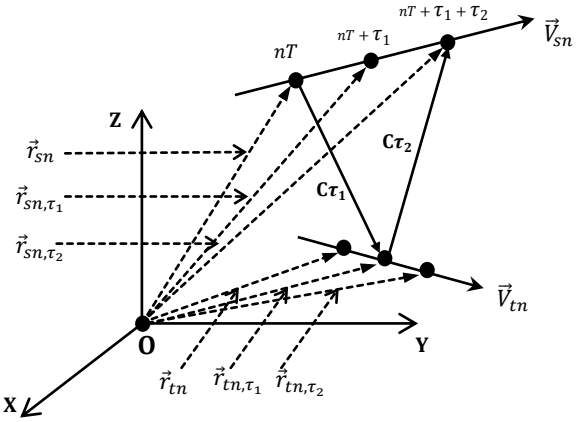

Fig. 2 GEO SAR propagation

$$R_n(t_r) = C\tau_1 + C\tau_2 \tag{4}$$

with:

$$\begin{aligned} R_{1n} &= C\tau_1 = \left\|\vec{r}_{sn} - \vec{r}_{tn,\tau_1}\right\| \\ R_{2n} &= C\tau_2 = \left\|\vec{r}_{tn,\tau_1} - \vec{r}_{sn,\tau_2}\right\| \end{aligned} \tag{5}$$

Developing R_{1n} and R_{2n} as a Maclaurin series with respect to the fast time, and replacing them into (4), the one-way range propagation signal will be:

$$\begin{aligned} r_n(t_r) = \frac{R_n(t_r)}{2} = \|\vec{r}_{sn} - \vec{r}_{tn}\| + \frac{1}{2}\left(\vec{V}_{sn} - \vec{V}_{tn}\right)\vec{U}_{st,n}{}^{T}.t_r \\ + \frac{\vec{V}_{sn}(\vec{V}_{sn}-\vec{V}_{tn})^T}{\|\vec{r}_{tn}-\vec{r}_{sn}\|}\frac{{t_r}^2}{8} + \frac{\vec{V}_{tn}\left(I-\vec{U}_{st,n}{}^{T}\vec{U}_{st,n}\right)\vec{V}_{tn}{}^{T}}{\|\vec{r}_{sn}-\vec{r}_{tn}\|}\frac{{t_r}^2}{16} \\ + \frac{1}{16}\left[\begin{array}{c}\frac{(\vec{V}_{sn}-\vec{V}_{tn})\left(I-\vec{U}_{st,n}{}^{T}\vec{U}_{st,n}\right)(\vec{V}_{sn}-\vec{V}_{tn})^T}{\|\vec{r}_{sn}-\vec{r}_{tn}\|} \\ + \frac{\vec{V}_{sn}(I-\vec{U}_{st,n}{}^{T}\vec{U}_{st,n})\vec{V}_{sn}{}^{T}}{\|\vec{r}_{sn}-\vec{r}_{tn}\|}\end{array}\right]{t_r}^2 \end{aligned} \tag{6}$$

$$\text{with : } \vec{U}_{st,n} = \frac{(\vec{r}_{sn}-\vec{r}_{tn})}{\|\vec{r}_{sn}-\vec{r}_{tn}\|},\ \vec{U}_{st,n,\tau_1} = \frac{(\vec{r}_{tn,\tau_1}-\vec{r}_{sn,\tau_1})}{\|\vec{r}_{tn,\tau_1}-\vec{r}_{sn,\tau_1}\|} \tag{7}$$

Likewise, we have:

$$\left\|\vec{r}_{tn,\tau_1} - \vec{r}_{sn,\tau_1}\right\| = \left\|(\vec{r}_{tn}-\vec{r}_{sn}) + (\vec{V}_{tn} - \vec{V}_{sn})\tau_1)\right\| \tag{8}$$

Replacing (8) into (6), and keeping $r_n(t_r)$ to the first order (short fast time), this yields:

$$r_n(t_r) = \underbrace{\|\vec{r}_{sn} - \vec{r}_{tn}\|}_{r_n(t_r)|_{stop\&go}} + \underbrace{\frac{1}{2}\left(\vec{V}_{sn} - \vec{V}_{tn}\right)\vec{U}_{st,n}{}^{T}.t_r}_{\Delta r_n(t_r)} \tag{9}$$

$$\text{where}\quad t_r = \frac{2.\|\vec{r}_{sn}-\vec{r}_{tn}\|}{c} \tag{10}$$

$$\Rightarrow \Delta r_n(t_r) = \frac{(\vec{V}_{sn}-\vec{V}_{tn})(\vec{r}_{sn}-\vec{r}_{tn})^T}{c} \tag{11}$$

After approximating $r_n(t_r)$ with a Maclaurin series with respect to the azimuth time (n), and replacing it into (3), we can deduce f_{DC} and f_{DR} as:

$$f_{DC} = -\frac{2}{\lambda}\left[\begin{array}{c}\frac{(\vec{V}_{s0}-\vec{V}_{t0})(\vec{r}_{s0}-\vec{r}_{t0})^T}{\|\vec{r}_{s0}-\vec{r}_{t0}\|} \\ + \frac{(\vec{a}_{s0}-\vec{a}_{t0})(\vec{r}_{s0}-\vec{r}_{t0})^T + (\vec{V}_{s0}-\vec{V}_{t0})(\vec{V}_{s0}-\vec{V}_{t0})^T}{c}\end{array}\right] \tag{12}$$

$$f_{DR} = \frac{2}{\lambda}\left(\begin{array}{c}\frac{(\vec{a}_{s0}-\vec{a}_{t0})(\vec{r}_{s0}-\vec{r}_{t0})^T + \|\vec{V}_{s0}-\vec{V}_{t0}\|^2}{\|\vec{r}_{s0}-\vec{r}_{t0}\|} \\ - \frac{\left[(\vec{V}_{s0}-\vec{V}_{t0})(\vec{r}_{s0}-\vec{r}_{t0})^T\right]^2}{\|\vec{r}_{s0}-\vec{r}_{t0}\|^3} \\ + \frac{(\vec{b}_{s0}-\vec{b}_{t0})(\vec{r}_{s0}-\vec{r}_{t0})^T + 3(\vec{a}_{s0}-\vec{a}_{t0})(\vec{V}_{s0}-\vec{V}_{t0})^T}{c}\end{array}\right) \tag{13}$$

The subscript '0' stands for the centre of the aperture. Equations (12) and (13) represent the new closed-form expressions of the Doppler parameters in the GEO SAR case.

We assume for simplicity a moving target with constant cross-track and along-track velocities, besides, the derivative of the satellite acceleration vector $\vec{b}_{s0}$ can be neglected. The satellite and target parameters are set as follows:

$$\vec{V}_{t0} = \begin{pmatrix} V_{tx0} \\ V_{ty0} \\ 0 \end{pmatrix}^T, \vec{r}_{s0} = \begin{pmatrix} x_{s0} \\ y_{s0} \\ z_{s0} \end{pmatrix}^T, \vec{r}_{t0} = \begin{pmatrix} x_{t0} \\ y_{t0} \\ z_{t0} \end{pmatrix}^T, \vec{V}_{s0} = \begin{pmatrix} V_{sx0} \\ V_{sy0} \\ V_{sz0} \end{pmatrix}^T$$

Using these parameters, the final expressions of f_{DC} andf_{DR}, after further developments and simplifications will be:

$$f_{DC} \approx \frac{2}{\lambda}\left[\underbrace{V_{tx0}\left[\frac{(x_{s0}-x_{t0})}{\|\vec{r}_{s0}-\vec{r}_{t0}\|}\right]}_{Target\ radial\ velocity} + V_{ty0}\left[\frac{(y_{s0}-y_{t0})}{\|\vec{r}_{s0}-\vec{r}_{t0}\|}\right]\right] \tag{14}$$

$$\underbrace{f_{DC}}_{GEO\ SAR} \approx \underbrace{f_{DC_L}}_{\substack{Doppler\ centroid \\ in\ LEO\ SAR}} + \underbrace{\frac{2}{\lambda}V_{ty0}\left[\frac{(y_{s0}-y_{t0})}{\|\vec{r}_{s0}-\vec{r}_{t0}\|}\right]}_{\substack{Stop\ and\ go\ error combined\ with \\ long\ integration\ time\ error}} \tag{15}$$

$$f_{DR} = \frac{2}{\lambda}\left[\begin{array}{c}\frac{(\vec{a}_{s0})(\vec{r}_{s0}-\vec{r}_{t0})^T}{\|\vec{r}_{s0}-\vec{r}_{t0}\|} + \frac{\vec{V}_{s0}\vec{V}_{s0}{}^{T}}{\|\vec{r}_{s0}-\vec{r}_{t0}\|} + \frac{\vec{V}_{t0}\vec{V}_{t0}{}^{T}}{\|\vec{r}_{s0}-\vec{r}_{t0}\|} \\ - \frac{{V_{ty0}}^2(y_{s0}-y_{t0})^2}{\|\vec{r}_{s0}-\vec{r}_{t0}\|^3} - V_{tx0}\frac{2V_{sx0}}{\|\vec{r}_{s0}-\vec{r}_{t0}\|} \\ + V_{ty0}\left[\frac{2(y_{s0}-y_{t0})\vec{V}_{s0}(\vec{r}_{s0}-\vec{r}_{t0})^T}{\|\vec{r}_{s0}-\vec{r}_{t0}\|^3} - \frac{2V_{sy0}}{\|\vec{r}_{s0}-\vec{r}_{t0}\|}\right]\end{array}\right] \tag{16}$$

We can notice from (14) and (16) that both Doppler centroid and Doppler rate depend on the target cross-track and along-track velocities, which is not the case in the LEO SAR scenario, where one could retrieve the target cross-track velocity having only the first order Doppler parameter, and where the Doppler rate is only function of the along-track velocity and the radial acceleration.

Furthermore, the factor $\frac{x_{s0}-x_{t0}}{\|\boldsymbol{r}_{s0}-\boldsymbol{r}_{t0}\|}$ that relates the cross-track velocity to the Doppler centroid is of the order of 1 (≈ 1), while the term $\frac{y_{s0}-y_{t0}}{\|\boldsymbol{r}_{s0}-\boldsymbol{r}_{t0}\|} \approx 10^{-1}$, which means that the impact of the Cross-track velocity on the Doppler centroid value is bigger than the along-track velocity.

To retrieve the target's motion parameters, we first use (14) to extract the expression of the cross-track velocity as follows:

$$V_{tx0} = \frac{c.\|\boldsymbol{r}_{s0}-\boldsymbol{r}_{t0}\|}{c(x_{s0}-x_{t0})-2V_{sx0}\|\boldsymbol{r}_{s0}-\boldsymbol{r}_{t0}\|}\left[\begin{array}{c}+\frac{\lambda}{2}f_{DC} + \frac{\boldsymbol{V}_{s0}(\boldsymbol{r}_{s0}-\boldsymbol{r}_{t0})^T}{\|\boldsymbol{r}_{s0}-\boldsymbol{r}_{t0}\|} \\ + \frac{\boldsymbol{V}_{s0}\boldsymbol{V}_{s0}{}^{T}}{c} + \frac{\boldsymbol{a}_{s0}(\boldsymbol{r}_{s0}-\boldsymbol{r}_{t0})^T}{c} \\ - V_{ty0}\left[\frac{(y_{s0}-y_{t0})}{\|\boldsymbol{r}_{s0}-\boldsymbol{r}_{t0}\|} - \frac{2V_{sy0}}{c}\right]\end{array}\right] \tag{17}$$

We then replace (17) into (16), and solve the second order polynomial function.

IV. DOPPLER PARAMETER ESTIMATION

After range compression of the SAR image, the azimuth signal is filtered using a high filter to delete the stationary target signal, then the output of the filter is used for the estimation of the motion parameters. To perform this task, several methods have been developed in the literature. P.

O'Shea introduces a Cubic Phase Function (CPF) in [13] for the estimation of the parameters of a 3rd order Polynomial Phase Signal (PPS), but this technique suffers from the need to perform a computationally demanding one dimensional search and unfits for a GEO SAR application. I. Djurovic et al. proposed the Hybrid CPF-HAF (High Ambiguity Function) technique in [14] based on the CPF, that considers higher order PPS, but still does not solve the computational issue. A modified version of the CPF-HAF has been proposed in [15] named Non Uniform CPF-HAF, which is computationally efficient. In this work, we approximated the GEO SAR signal by a third order PPS so we can avoid computing the HAF step that increases the SNR threshold by 6 dB [14]. This approximation is quite good, since the 4th order coefficient is rather small and does not impact the estimation accuracy of lower parameters. For a 3rd order signal:

$$x(n) = exp(j\sum_{i=1}^{3} a_i\,(nT)^i)\,, -\frac{N}{2} < n < \frac{N}{2} \tag{18}$$

where $(N+1)$ is the number of azimuth samples, $T = \frac{1}{PRF}$, is the PRI. The NU-CPF is defined as follows:

$$NUCPF(n_a, \Omega) = \sum_k \begin{Bmatrix} S\left(n_a + \sqrt{Ck}\right).S\left(n_a - \sqrt{Ck}\right) \\ .exp(-j\Omega C T^2 k) \end{Bmatrix} \tag{19}$$

Where C is a sampling factor, (19) can be further expanded as:

$$NUCPF(n, \Omega) = \sum_k \underbrace{exp\begin{Bmatrix} j((6a_3nT + 2a_2)T^2Ck + 2a_3(nT)^3 \\ +2a_3(nT)^2 + a_1nT) \end{Bmatrix}}_{x_1(k)} .exp(-j\Omega T^2 Ck)$$
$$= FT\{x_1(k)\} \tag{20}$$

Which is no more than a Fourier transform of $x_1(k)$.
The NUCPF has its maximum at:

$$\Omega(n) = 6a_3nT + 2a_2 \tag{21}$$

So if we evaluate $NUCPF(n, \Omega)$ at two different azimuth times $t_1 = n_1T$ and $t_2 = n_2T$, we can deduce the values of a_2 and a_3 from the corresponding Fourier transform's peaks. Having a_2 and a_3, after dechirping the original signal, we get:

$$x(n) = exp\big(j(a_1nT)\big)\,, -\frac{N}{2} < n < \frac{N}{2} \tag{22}$$

where the last parameter a_1 can be retrieved from the peak of the complex sinusoid spectrum.

V. Simulation Results

In order to validate the efficiency of the proposed method, we run some simulations, we kept the same GEO SAR parameters used earlier to simulate an echo from a moving target and a stationary target, the moving target evolves with different cross-track and along-track velocities, that correspond to three different scenarios in order to see the effect of either velocities on the Doppler parameters f_{Dc} and f_{DR}. The Doppler parameters estimation and the corresponding estimated motion velocities are presented in Table III.

We can see that the proposed method is able to accurately estimate the target's motion parameters in the three scenarios. Moreover, we notice from scenarios S1 and S2, that the Doppler centroid depends more on the cross-track velocity than it depends on the along-track velocity as deduced from (14).

TABLE III. PARAMETERS ESTIMATION RESULTS

Parameters	S1	S2	S3
True $V_{tx0}\ (m/s)$	20	20	0
True $V_{ty0}\ (m/s)$	20	0	20
Estimated $V_{tx0}\ (m/s)$	20.00	20.00	0
Estimated $V_{ty0}\ (m/s)$	19.99	−0.00009	20.00
Estimated V_{tx0} using Classical Doppler centroid expression (m/s)	20.68	19.99	0.68
$f_{DC}\ (Hz)$	161.19	155.86	5.32
$f_{DR}\ (Hz/s)$	−0.0415	−0.0427	−0.0415

On the other hand, we notice that the Doppler rate is more sensitive to the variation of the along-track velocity than the cross-track velocity as can be deduced from scenarios S1 with S3, and S2 with S3. This is due to the fact that the along-track velocity in the last term of (16) is multiplied with the satellite along-track velocity ($\approx 119\ m/s$), which enhances its effect on the Doppler rate, whereas the cross-track velocity is multiplied by the satellite cross-track velocity which is small ($\approx 5\ m/s$), hence, resulting in a small cross-track velocity effect on the Doppler rate. These results confirm the theoretical observations drawn in section II.

Moreover, we can see the difference between the estimation of the moving target cross-track velocity using the classical Doppler centroid expression (no along-track velocity involved), and the new developed expression, in fact, the use of the new GEO SAR expression results in a better estimate, whereas, the classical expression induces an error proportional to the target along-track velocity (see (15)).

VI. Conclusion

GEO SAR systems present a great potential in term of global mapping, due to their short revisit time (1 day) [16] and high altitude orbit (36500 km)[17]. However, these GEO SAR characteristics undermine the classical equations that describe the imaging process of actual airborne and space-borne SAR systems.

In this paper, we developed new closed-form expressions for the Doppler parameters in GEO SAR, based on these formulations, we proposed the use of the NUCPF algorithm to estimate the moving target motion velocities. Finally, some simulations were conducted to demonstrate the efficiency of the proposed technique.

Acknowledgment

This work was supported by the National Natural Science Foundation of China (Grant Nos. 61501032, 61471038 and 61427802), 111 project (Grant No. B14010).

References

[1] S. N. Madsen, W. Edelstein, L. D. DiDomenico, and J. LaBrecque, "A geosynchronous synthetic aperture radar; for tectonic mapping, disaster management and measurements of vegetation and soil moisture," *Geosci. Remote Sens. Symp. 2001. IGARSS '01. IEEE 2001 Int.*, vol. 1, no. 2, pp. 447–449 vol.1, 2001.

[2] S. N. Madsen, C. Chen, and W. Edelstein, “Radar Options for Global Earthquake Monitoring,” vol. 0, no. C, pp. 1483–1485, 2002.

[3] D. Cerutti-Maori, I. Sikaneta, and C. H. Gierull, “Optimum SAR/GMTI processing and its application to the radar satellite RADARSAT-2 for Unitoring,” *IEEE Trans. Geosci. Remote Sens.*, vol. 50, no. 10 PART1, pp. 3868–3881, 2012.

[4] J. H. G. Ender, “Space-time processing for multichannel synthetic aperture radar,” *Electron. Commun. Eng. J.*, vol. 11, no. 1, p. 29, 1999.

[5] M. Ruegg, E. Meier, and D. Nuesch, “Capabilities of Dual-Frequency Millimeter Wave SAR With Monopulse Processing for Ground Moving Target Indication,” *Geosci. Remote Sensing, IEEE Trans.*, vol. 45, pp. 539–553, 2007.

[6] C. Gierull and I. C. Sikaneta, “Raw data based two-aperture SAR ground moving target indication.” pp. 1032–1034 vol.2, 2003.

[7] E. Chapin and C. W. Chen, “Airborne along-track interferometry for GMTI,” *Aerosp. Electron. Syst. Mag. IEEE*, vol. 24, pp. 13–18, 2009.

[8] D. Henke, E. Mendez Dominguez, D. Small, M. E. Schaepman, and E. Meier, “Moving Target Tracking in Single- and Multichannel SAR,” *IEEE Trans. Geosci. Remote Sens.*, vol. 53, no. 6, pp. 3146–3159, 2015.

[9] C. Hu, F. Liu, W. Yang, T. Zeng, and T. Long, “Modification of slant range model and imaging processing in geo SAR,” *Int. Geosci. Remote Sens. Symp.*, pp. 4679–4682, 2010.

[10] C. Hu, T. Long, Z. Liu, T. Zeng, and Y. Tian, “An improved frequency domain focusing method in geosynchronous SAR,” *IEEE Trans. Geosci. Remote Sens.*, vol. 52, no. 9, pp. 5514–5528, 2014.

[11] M. Eineder, H. Runge, E. Boerner, R. Bamler, N. Adam, B. Schättier, H. Breit, and S. Suchandt, “SAR interferometry with TERRASAR-X,” *Eur. Sp. Agency, (Special Publ. ESA SP*, vol. 2003, no. 550, pp. 289–294, 2004.

[12] C. Hu, T. Long, T. Zeng, F. Liu, and Z. Liu, “The accurate focusing and resolution analysis method in geosynchronous SAR,” *IEEE Trans. Geosci. Remote Sens.*, vol. 49, no. 10 PART 1, pp. 3548–3563, 2011.

[13] P. O’Shea, “A fast algorithm for estimating the parameters of a quadratic FM signal,” *IEEE Trans. Signal Process.*, vol. 52, no. 2, pp. 385–393, 2004.

[14] I. Djurović, M. Simeunović, S. Djukanović, and P. Wang, “A hybrid CPF-HAF estimation of polynomial-phase signals: Detailed statistical analysis,” *IEEE Trans. Signal Process.*, vol. 60, no. 10, pp. 5010–5023, 2012.

[15] M. Simeunović and I. Djurović, “Non-uniform sampled cubic phase function,” *Signal Processing*, vol. 101, pp. 99–103, 2014.

[16] K. Tomiyasu and J. L. Pacelli, “Synthetic Aperture Radar Imaging from an Inclined Geosynchronous Orbit,” *IEEE Trans. Geosci. Remote Sens.*, vol. GE-21, no. 3, pp. 324–329, 1983.

[17] C. Hu, T. Long, and Y. Tian, “an Improved Nonlinear Chirp Scaling Algorithm Based on Curved Trajectory in Geosynchronous Sar,” *Prog. Electromagn. Res.*, vol. 135, no. June 2017, pp. 481–513, 2013.